Coiling, Entrainment, and Hydrodynamic Coupling of Decelerated Fluid Jets

Christopher Dombrowski,[1] Braddon Lewellyn,[1] Adriana I. Pesci,[1] Juan M. Restrepo,[1,2,3]
John O. Kessler,[1] and Raymond E. Goldstein[1,2]

[1]*Department of Physics, University of Arizona, Tucson, Arizona 85721, USA*
[2]*Program in Applied Mathematics, University of Arizona, Tucson, Arizona 85721, USA*
[3]*Department of Mathematics, University of Arizona, Tucson, Arizona 85721, USA*

(Received 11 August 2004; published 28 October 2005)

From algal suspensions to magma upwellings, one finds jets which exhibit complex symmetry-breaking instabilities as they are decelerated by their surroundings. We consider here a model system—a saline jet descending through a salinity gradient—which produces dynamics unlike those of standard momentum jets or plumes. The jet coils like a corkscrew within a conduit of viscously entrained fluid, whose upward recirculation braids the jet, and nearly confines transverse mixing to the narrow conduit. We show that the underlying jet structure and certain scaling relations follow from similarity solutions to the fluid equations and the physics of Kelvin-Helmholtz instabilities.

DOI: 10.1103/PhysRevLett.95.184501 PACS numbers: 47.20.−k, 47.54.+r, 92.10.−c, 95.30.Lz

The broad range of physical and biological systems which exhibit fluid jets and plumes often display symmetry-breaking instabilities as the injected fluid interacts viscously with its surroundings. Examples include helical jets outflowing from a galactic nucleus [1], upwelling magma conduits [2], plumes from hydrothermal vents [3], and filamentary downwellings in algal suspensions [4]. Key issues in all are mixing and entrainment by the jet and the nonlinear regime far beyond the instabilities. Here we study a jet, which, unlike momentum jets (e.g., the Bickley jet [5]), has a different density than the surrounding fluid, which in turn is stratified. Specifically, we study a fluid jet that decelerates by descent through a linear density gradient, differing from the surround only by the concentration of the solute that defines the gradient. This system operates at modest Reynolds numbers, quite distinct from turbulent plumes such as smoke stacks, effluent discharges, and volcanic eruptions [6]. In our system, the dynamics of single jets and pairs derive from a complex flow field created as they penetrate the gradient (Fig. 1), organized around a *conduit* of entrained fluid [2,7,8] braiding the jet, supporting wavelike or singular excitations on its wall [9]. This conduit is composed primarily of fresher water, visible by its index contrast with the stratified surroundings. We show that the coiling instability is a bifurcation which can be understood through similarity solutions of the fluid equations and the physics of Kelvin-Helmholtz instabilities. Like coordinated flapping of nearby filaments in a flowing soap film [10] which depends strongly on their separation, we also find coupled, synchronized coiling which varies with the separation of nearby jets.

An experimental control parameter is the flux Q of the pump driving the flow or the average velocity $u = Q/\pi a^2$ of the fluid exiting the nozzle of radius a. Over the range studied $0.02 \leq Q \leq 5$ cm^3/hr (0.003 cm/s $\leq u \leq$ 0.7 cm/s) and with $\nu = 0.01$ cm^2/s the kinematic viscosity of water, the jet Reynolds number is $\mathrm{Re} = ua/\nu \sim$ 0.01–2, well in the laminar regime. The diffusion constant of salt $D = 1.5 \times 10^{-5}$ cm^2/s gives a Schmidt number $\mathrm{Sc} = \nu/D \sim 10^3$; mechanical dissipation dominates diffusion, and the Peclet number $\mathrm{Pe} = \mathrm{Re} \times \mathrm{Sc}$ is very large, so advection also dominates diffusion. This latter aspect, the stratification, and finite Reynolds number effects together make this problem unlike pure momentum jets or diffusive plumes. A jet introduced into the fluid produces a steady

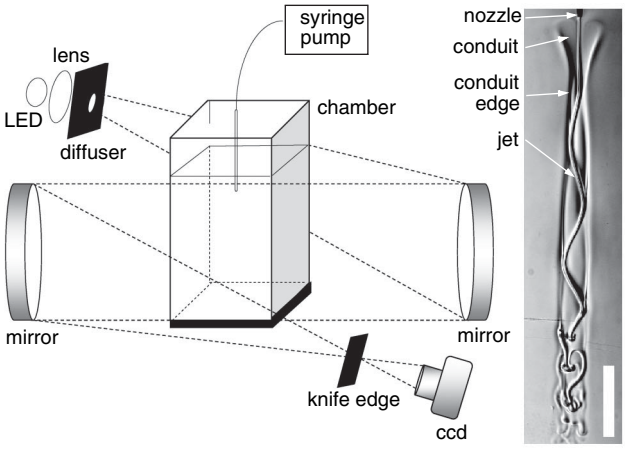

FIG. 1. Left: Each half of the stereoscopic Schlieren system has 6-inch $F/10$ parabolic mirrors, light-emitting diode illumination, and a knife edge at the focus. 12 bit digital CCD cameras (Hamamatsu C7300) with 80–200 mm $f/2.8$ lenses acquire images to a personal computer. The chamber is a parallelipiped $18 \times 18 \times 61$ cm of 6 mm plate glass. Jets exit a nozzle of radius $a = 0.025$ cm attached to a syringe pump (New Era Pump Systems N1000). Salinity gradients were produced by the "two-bucket" method, measured *in situ* by suspending 5 mm floats (American Density Materials). Particle imaging velocimetry was performed with a He-Ne laser sheet, suspended microspheres (Sphericel, Potters Ind., $\rho = 1.1$ g/cm^3, mean diameter 11.7 μm), and software analysis (Dantec). Right: Flow features, with 5 mm scale.

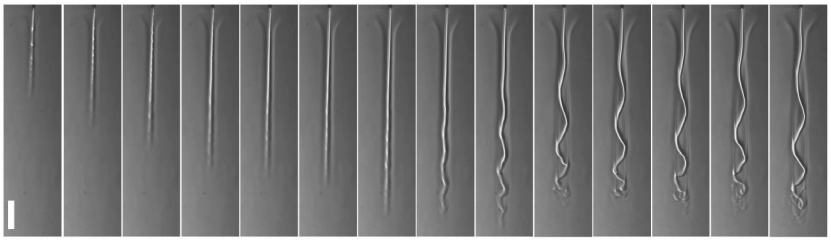

FIG. 2. Coiling instability. With increasing velocity (see Fig. 3), the jet penetrates further into the gradient and then coils. Bar is 5 mm.

conduit in 5–10 s, as entrained flow builds around the jet through vorticity diffusion. The conduit edge, clearly seen in Fig. 1, has a width $\lesssim 0.01$ cm. The jet, inside the conduit, remains straight until the velocity exceeds a critical value u^*, beyond which it becomes helical (Fig. 2). The conduit hugs a straight jet tightly beyond ~ 5 mm below the nozzle but flares out closer. When coiling begins, the conduit widens so the jet is inscribed on it, like the buckling of constrained elastica [11]. The frequency f, wavelength λ, and wave speed c are finite at u^*, increasing slowly beyond [Figs. 3(c) and 3(d)].

Consider first the regime $u < u^*$ and the *termination length* z^*, the distance between the injector and the location at which image analysis can no longer differentiate the jet from its surroundings. Even when the jet density exceeds that of the surroundings at the chamber bottom, z^* is much less than the overall fluid depth H, so diffusional spreading of the jet clearly diminishes its density as it descends. Apart from an offset at small u, Fig. 3(a) shows that $z^* \sim u^{1/2}$, and, apart from a transition zone very near the nozzle, the jet width collapses onto a common *line* versus z/z^* [Fig. 3(b)]. To explain these results, consider an incompressible axisymmetric flow $\mathbf{u}(r, z) = u(r, z)\hat{\mathbf{z}} + v(r, z)\hat{\mathbf{r}}$ and salt concentration $S(r, z)$. For a slender jet, the leading terms in the Navier-Stokes and advection-diffusion equations are [12,13]

$$u\frac{\partial u}{\partial z} + v\frac{\partial u}{\partial r} = \nu\frac{1}{r}\frac{\partial}{\partial r}\left(r\frac{\partial u}{\partial r}\right) + g\kappa S, \tag{1}$$

$$u\frac{\partial S}{\partial z} + v\frac{\partial S}{\partial r} = D\frac{1}{r}\frac{\partial}{\partial r}\left(r\frac{\partial S}{\partial r}\right), \tag{2}$$

where the constant κ relates salinity and density changes. Far from the jet, the salinity asymptotes to the gradient: $\lim_{r\to\infty} S(r, z) = S_0 + S_G z/H$. If S_j is the jet salinity, the existence of a *stratification length* $\ell_G = (S_G/S_j)H$ eliminates the possibility that (1) and (2) possess a strict similarity solution. Since $\ell_G \gg z^*$, we explore the notion of a *local similarity* solution to (1) and (2) in the absence of a gradient. Computing the velocity from a stream function, $u = (1/r)\partial\psi/\partial r$ and $v = -(1/r)\partial\psi/\partial z$, we propose

$$\psi = \nu z^\alpha f(\xi), \qquad S = \frac{\nu^2}{g} d^4 z^\delta \phi(\xi), \qquad \xi = d\frac{r}{z^\beta}. \tag{3}$$

The dimensionless factor d is found below. Equations (1) and (2) reduce to ordinary differential equations if $\alpha = 1$ and $\delta = \alpha - 4\beta$. Unlike free diffusion [12,13], here, as in the Bickley jet [5], the nozzle is a source of momentum, whose conservation constrains the exponents. For the momentum flux $M \sim \int dr r u^2 \sim z^{2(\alpha-\beta)} \int d\xi (f'^2/\xi)$ to be conserved, the z dependence must vanish, yielding $\beta = 1$, $\delta = -3$.

Define the edge of the jet by the radius r_j at which S is some fraction of its center line value, hence at some $\xi = \tilde{\xi}$. With $\beta = 1$, the edge is the straight line $r_j = (\tilde{\xi}/d)z$, like the data in Fig. 3(b), but the role of z^* in collapsing the data is not yet shown. We can find d by noting [13] that, if at some z_0 we know the flux Q and integrated salt concentration C, then the similarity solutions yield $Q = 2\pi\nu z_0 f(\infty)$ and $C = 2\pi d^4(\nu^2/g z_0)\int d\xi \xi\phi$. Hence, $d \sim Q^{1/2}(\Delta\rho_j)^{1/2}$, where $\Delta\rho_j$ is the density difference between the jet and pure water. We hypothesize that z^* can be found

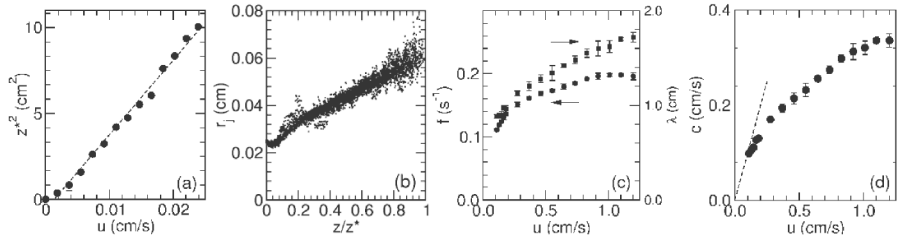

FIG. 3. Jet data. (a) Square of the termination length z^* versus nozzle velocity, showing linear relationship. (b) Jet width r_j as a function of z/z^*. Oscillations near $z/z^* \sim 1$ show emergence of an axisymmetric instability; deviations at small z/z^* reflect the influence of the flaring conduit. Coiling frequency and wavelength (c) and wave speed (d) as functions of jet velocity. In (d), the dashed line is the identity expected from the Kelvin-Helmholtz physics, which is accurately obeyed at onset.

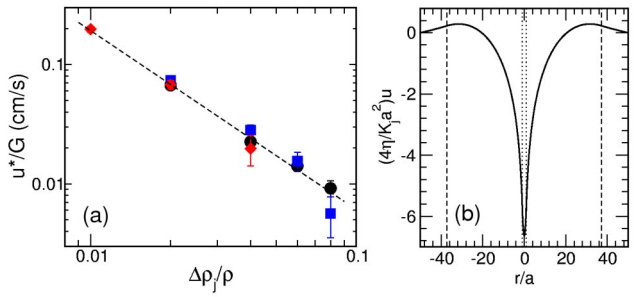

FIG. 4 (color online). (a) Critical buckling velocity as a function of the relative density offset of the jet, rescaled by dimensionless gradient: $G = 2$ (black circles), $G = 1$ (blue squares), and $G = 0.5$ (red diamonds). (b) Velocity profile in 3-fluid model, with jet (dotted line) and conduit (dashed line) locations shown.

from the difference ΔS between the falling salinity at the jet center line, computed from the similarity solution, and the rising salinity of the background,

$$\Delta S \sim \frac{\nu^2 d^4 \phi(0)}{g z^3} - S_G \frac{z}{H}. \tag{4}$$

When $\Delta S = 0$, the descending jet terminates at $z^* \sim d$. Using the above results for d, we conclude also $z^* \sim Q^{1/2}(\Delta\rho_j)^{1/2}$, the dependence on Q (hence on u) being in agreement with data in Fig. 3(a). The half-width of the jet thus obeys a scaling form, $r_j \sim z/z^*$ independent of the flux Q, consistent with the data [Fig. 3(b)].

The coiling instability exhibits a scaling law for the buckling velocity $u^*/G \sim (\Delta\rho_j)^{-\gamma}$, with $\gamma \sim 1.5$ [Fig. 4(a)], where G is the dimensionless maximum salinity in the gradient, S_G, measured in M/l. We find that an explanation for this centers around the flow field in the conduit. Particle imaging velocimetry (PIV) analysis [Fig. 5(a)] reveals that there is a strong return flow within the conduit and small flow beyond it. A simple model of this involves *three* fluids: a jet of radius a, density ρ_j, a conduit of radius b with pure water, within a surround of density ρ_s in a cylindrical tank of radius R. Assuming near-parallelism of the flow and solving $\nabla^2 u_i(r) = K_i$, with $K_i = (\partial p_i/\partial z + \rho_i g)/\eta$ in each domain, with continuity in velocity and viscous stress at the two interfaces, we obtain the full flow field. For a given jet radius a and parameters $\{K_i\}$, the conduit radius b follows from mass conservation. Using representative parameters, Fig. 4(b) shows the very strong velocity gradient within the conduit and the clear return flow along the outer edge and beyond. The relative smallness of the velocity at the conduit edge implies that this geometry is akin to two-phase pipe flow with a no-slip boundary condition at the wall: the "core-annular" flow of lubricated pipelines [14], the inner jet playing the role of the oil, the outer fluid, the water. Stability analysis for that flow shows that, when $b \gtrsim 1.2a$, the most unstable mode is helical with wavelength $\lambda \sim 7.5b$ [15], and the axisymmetric mode is also unstable. That $\lambda \sim b$ is expected, since the width of the shear layer sets the scale of the unstable mode [16]. Although this coiling is superficially similar to that of a viscous jet impinging on a surface [17–19], it is distinguished by the role of shear.

We propose that the coiling instability occurs when the advected vertical momentum flux balances the radial flux, $u^2/\lambda \sim v^2/a$. The similarity solution yields $v/u \sim d \sim (\Delta\rho_j Q)^{1/2}$, and the three-fluid model shows that, when the outer fluid is in hydrostatic equilibrium ($K_s = 0$) and the container is large ($R/a \gg 1$), then $b/a \simeq [(\rho_j - \rho_s)/(\rho_s - \rho_c)]^{1/2}$. Evaluating this at $z = z^*$ and using $\lambda \sim b$, we find $Q^* \sim (\Delta\rho_j)^{-3/2}$, in agreement with the results in Fig. 4(a). In shear-driven instabilities, the wave speed c is generally the velocity at the junction between the two opposing flows. Identifying that point with the edge of the jet, Fig. 4(b) shows that the velocity there is just slightly less than the average velocity u in the jet. The data in Fig. 3(d) show that c is indeed very nearly equal to u near the instability onset, deviating downward at much higher velocities. This would appear to follow from the ever larger backflow in the conduit.

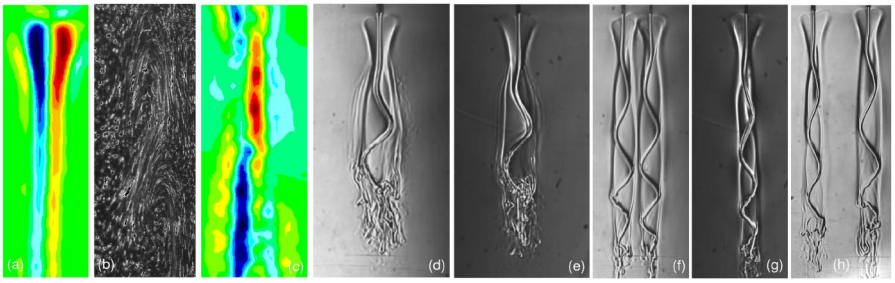

FIG. 5 (color online). Flow imaging and measurement. (a) PIV-derived toroidal vorticity near nozzle, averaged over many coiling periods, showing opposite senses of recirculation on either side of jet. (b) Streak image of suspended microspheres in the strongly coiled regime, (c) vorticity map in coiled regime, about one half-period shifted from (b). (d),(e) Front and side views, respectively, of two separate jets which have merged inside a shared conduit; (f) front and (g) side views of two nearby jets which synchronize as mirror images, and (h) front view of distant nested jets.

Using suspended microspheres, we obtained both streak images and vorticity (from PIV) of a coiled jet. The streak image in Fig. 5(b) shows the jet is *braided by a helical vortex*; when visualized in cross section, regions of clockwise and counterclockwise circulation appear to alternate down the jet [Fig. 5(c)], analogous to flows in the serpentine instability of two-dimensional plumes [20]. The circulation in the conduit—down along the jet, up at the conduit edge—is shown by the vorticity in Fig. 5(a), averaged over several periods, consistent with the model profile in Fig. 4. The coupling between nearby jets expected from these flows was studied with an apparatus which holds two nozzles at a variable center line separation s, each fed from a syringe pump. If nearly touching, the two jets share a single conduit, appearing almost as one from the front [5(d)] or side [5(e)]. If farther apart, yet closer than a conduit diameter, the dynamics (not shown) is unsteady. Once the separation exceeds a conduit diameter, there is striking synchronization of phase; from the front [5(f)] the jets are mirror images, while from the side [5(g)] they are perfectly aligned. Beyond a critical separation s^* which varies with velocity ($s^* \sim 10$ mm for $u \sim 5$ mm/s), the jets instead are *nested* [5(h)] and exhibit slow oscillations in the width of their conduits.

These complex coupled dynamics may arise from competing viscous and inertial effects. Studies of elastic sheets with sinusoidal traveling-wave deformations [21] and rotating rigid helices [22,23] show that the rate of viscous dissipation is greatly reduced in nested configurations, with their smaller velocity gradients. Although minimization of dissipation is not, in general, a mechanical driving force, it might explain why, at least at large separations, the jets arrange themselves to be nested [Fig. 5(h)]. It would not appear to explain why the two jets adopt mirror-image configurations when close. A possible explanation for the latter stems from the fact that the Reynolds number in this regime is on the order of unity, so inertial effects may compete with dissipation. When the jets are precisely out of phase, as in Fig. 5(f), the fluid in the regions of closest approach of the jets flows rapidly, reducing the pressure there through the Bernoulli effect, possibly driving the jets together. A detailed theory of these effects remains an open problem.

The complex flow fields shown here arise from remarkably simple ingredients—a saline fluid jet descending into density-stratified surroundings—which produce a conduit with counterpropagating shear flow, dynamical instabilities, and coupling between nearby jets. The dynamics neither conforms exclusively to standard momentum jet nor plume conceptualizations. With small modifications, this experiment can include baroclinic effects, providing a simple model to address mixing in oceanic flows, such as gravity currents along undersea canyons [24].

We thank J. W. Beck, R. Daly, L. Mahadevan, K. Visscher, and W. R. Young for discussions. This work was supported by NSF CTS0079725 and PHY0219411.

[1] A. P. Lobanov and J. A. Zensus, Science **294**, 128 (2001).
[2] J. A. Whitehead and K. R. Helfrich, Nature (London) **336**, 59 (1988).
[3] P. A. Rona, K. G. Bemis, D. Silver, and C. D. Jones, Mar. Geophys. Res. **23**, 147 (2002).
[4] J. O. Kessler, J. Fluid Mech. **173**, 191 (1986).
[5] P. G. Drazin and W. H. Reid, *Hydrodynamic Stability* (Cambridge University Press, Cambridge, England, 1981).
[6] J. S. Turner, *Buoyancy Effects in Fluids* (Cambridge University Press, Cambridge, England, 1973).
[7] K. R. Helfrich and J. A. Whitehead, Geophys. Astrophys. Fluid Dyn. **51**, 35 (1990).
[8] A. R. Tenner and B. Gebhart, Int. J. Heat Mass Transf. **14**, 2051 (1971).
[9] A. I. Pesci, M. A. Porter, and R. E. Goldstein, Phys. Rev. E **68**, 056305 (2003).
[10] J. Zhang, S. Childress, A. Libchaber, and M. Shelley, Nature (London) **408**, 835 (2000).
[11] G. Domokos, P. Holmes, and B. Royce, J. Nonlinear Sci. **7**, 281 (1997).
[12] T. Fujii, Int. J. Heat Mass Transf. **6**, 597 (1963).
[13] R. S. Brand and F. J. Lahey, J. Fluid Mech. **29**, 305 (1967).
[14] D. D. Joseph, R. Bai, K. P. Chen, and Y. Y. Renardy, Annu. Rev. Fluid Mech. **29**, 65 (1997).
[15] H. H. Hu and N. Patankar, J. Fluid Mech. **290**, 213 (1995).
[16] T. E. Faber, *Fluid Dynamics for Physicists* (Cambridge University Press, Cambridge, England, 1995).
[17] G. I. Taylor, in *Proceedings of the 12th International Congress on Applied Mechanics* (Stanford University, Stanford, 1968), p. 382.
[18] L. Mahadevan, W. S. Ryu, and A. D. T. Samuel, Nature (London) **392**, 140 (1998).
[19] N. M. Ribe, Phys. Rev. E **68**, 036305 (2003).
[20] J. R. Lister, J. Fluid Mech. **175**, 413 (1987).
[21] G. Taylor, Proc. R. Soc. A **209**, 447 (1951).
[22] M. Kim *et al.*, Proc. Natl. Acad. Sci. U.S.A. **100**, 15 481 (2003).
[23] M. Kim and T. R. Powers, Phys. Rev. E **69**, 061910 (2004).
[24] R. H. Kase, J. B. Girton, and T. B. Sanford, J. Geophys. Res. **108**, 3181 (2003).